A Simple Method for Tree Fall Detection on Medium Voltage Overhead Lines With Covered Conductors

Jan Fulneček and Stanislav Mišák

***Abstract*—Covered conductors are an alternative to aluminum core steel reinforced medium voltage overhead lines in forested terrains. The covered conductors are highly reliable due to the XLPE insulation system, which prevents the short-circuit current in case of contact of phases with the surrounding vegetation. However, the disadvantage of the covered conductor operation is the problematic detection of high impedance faults. Such type of faults is usually caused by the surrounding vegetation. The covered conductor may get ruptured or damaged due to the destructive degradation of the insulation system during the high impedance fault. This article contains a description and results of a new fault detection system for medium voltage overhead lines with covered conductors. The method of insulation fault identification is based on partial discharge activity detection. Our aim is to develop cheap and reliable online detector, which could be installed in large quantities for optimal high impedance fault detection and localization. Common partial discharges detectors are too expansive for this purpose.**

***Index Terms*—Partial discharges, Receiving antennas, Electromagnetic interference, Power distribution faults, Power distribution lines.**

Fig. 1. Fallen tree on medium voltage overhead line with covered conductors.

I. Introduction

THE biggest disadvantage of using covered conductors (CC) on medium voltage (MV) overhead lines is the problematic detection of high impedance faults (HIFs). When the surface of CC gets into the direct contact with an object of a different electric potential (usually surrounding vegetation or another CC), partial discharges (PD) appear on the surface of the CC covering and the fault current starts to flow through. The detection of HIF is difficult because of a very low value of the fault current [1]. The starting element of the standard digital relay protection cannot detect this type of faults. In the long-term, a partial discharge activity will lead to a failure of insulation, creating short circuit connection or earth fault [1], [2]. Fig. 1 shows a fallen tree on a MV overhead line with CC. After several days of PD activity, CC insulation burned through and the earth fault occurred. As clear from the photo, the earth fault current set the tree on fire. This is very dangerous, particularly in forested areas. This phenomenon is subject of extensive research [3]–[5].

The presence of PD activity is generally accepted as reliable tool for online monitoring of MV insulation system and it can be applied on overhead powerlines with CC. In such case, the high frequency content PD pattern is usually measured by Rogowski coils or various capacitive sensors [6]–[8]. Output voltage of Rogowski coil is proportional to the magnetic field strength near the surface of conductor. Acquired signals may be processed e.g. by wavelet transformation and can be classified by several ways [9]–[11].

To detect HIFs, a new device for PD detection on MV overhead lines with CC was developed at the VSB university. This device is used to detect branches and tree falls on the overhead line. It can detect PD activity which accompanies the phenomenon of the HIF (usually caused by the contact of CC with the surrounding vegetation). The detector uses three single layer inductors (SLI) as sensors; one sensor per one phase conductor. Unlike Rogowski coil, SLI is sensitive to the electric field strength (it creates capacitance coupling to the CC). This detector is already in use in more than 100 locations in the Czech Republic and has good results [12]. However, its price slows down its installation in other locations.

II. Motivation

To decrease the detector's price as low as possible, we decided to test the idea of replacing three SLI sensors with just one whip antenna sensor. There are several reasons why to do this.

Manuscript received January 24, 2020; revised May 11, 2020; accepted June 16, 2020. Date of publication July 10, 2020; date of current version May 21, 2021. This work was supported in by the following projects: Technology Agency of the Czech Republic - Projects TN01000007, TJ02000157 and TJ02000031, Students Grant Competition SP2020/127, project CZ.1.05/2.1.00/19.0389: Development of the ENET Center research infrastructure and LO1404: Sustainable Development of Center ENET. *(Corresponding author: Jan Fulneček.)*

The authors are with the Faculty of Electrical Engineering and Computer Science, VSB – Technical University of Ostrava, Ostrava 70800, Czech Republic (e-mail: jan.fulnecek@vsb.cz; stanislav.misak@vsb.cz).

Color versions of one or more of the figures in this article are available online at https://ieeexplore.ieee.org.

Digital Object Identifier 10.1109/TPWRD.2020.3008482

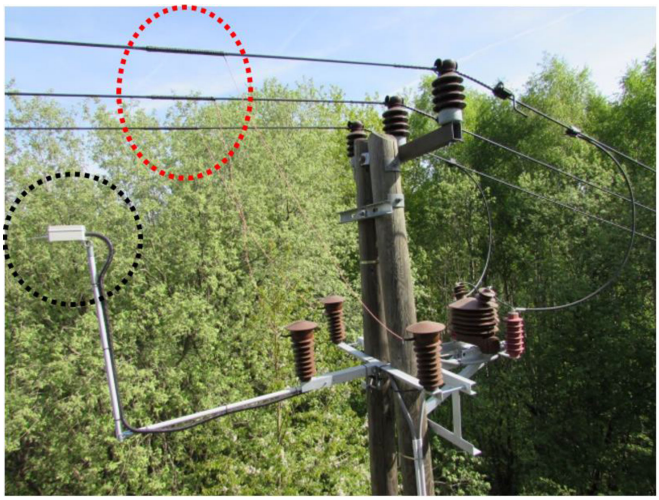

Fig. 2. Testing platform with BONIWhip antenna (black circle) and SLIs (red circle).

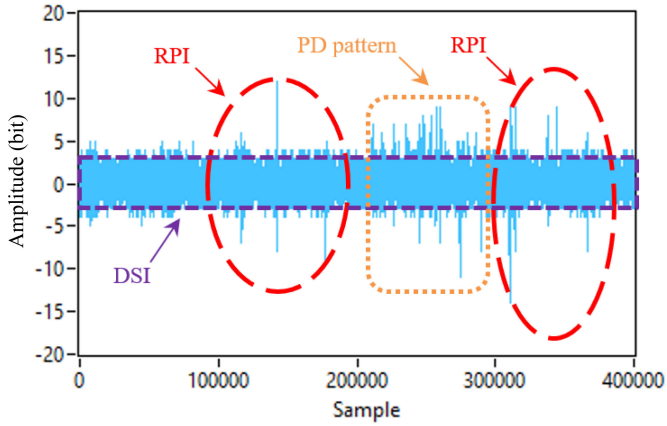

Fig. 3. DSI and RPI noise in acquired signal during HIF.

Unlike SLI, antenna sensor can be easily installed on an existing overhead line without any modifications of CC itself. It can also be installed without disconnecting the overhead line because it is a contactless sensor. A detector with SLI sensors requires 3 DAQ channels, while a detector with antenna sensor requires only a single channel DAQ. This also significantly decreases requirements for wireless data transmission. On the top of that, antenna sensor does not require a MV capacitive divider for its operation, unlike the SLI.

All these ideas have led us to construct a testing platform equipped with an antenna sensor besides SLIs (it is described in more details in [13]). This article presents the next step of this HIF detection method development – the simple algorithm for PD pattern recognition in acquired antenna signals.

III. Data Acquisition Description

To develop an algorithm, data from the testing platform were gathered. This testing platform was installed on the MV overhead line situated in the near the town of Krnov. The total length of examined power line is 12 km and the cross section is 50 mm^2. Testing platform is situated approximately in the middle of the power line and its range depends on the intensity of the PD activity. This location was chosen based on the harsh weather conditions and surrounding forested terrain, where higher fault rates can be expected. The whole measuring platform for PD detection is mounted on the pole of overhead line. It is in a box at the base of pole and it contains a power source with a backup battery, DAQ with 20 MS/s sample rate and control unit. This enables us to examine signals in a frequency spectrum up to 10 MHz. Antenna sensor is mounted on the stick approximately 50 cm below CC (see Fig. 2) and connected to DAQ.

Boni-Whip antenna was used as an antenna sensor. It is a common type of a wideband whip antenna with compact dimensions and low price. Data from the antenna sensor were gathered, while SLI sensors were used for data verification and annotation. This enabled us to verify the results of detection with antenna sensor.

Every hour, the antenna output signal is acquired in a length of 20 ms (acquired length is equal to the period of 50 Hz power grid system). Acquired data are transferred through GSM network to the server for classification. In total, 26660 signals (signal represents 20 ms period and consists of 400000 samples) were acquired during three years to validate the detection results.

IV. Acquired Signals Description

Unlike under the laboratory conditions, the acquired signals from a real environment contain high levels of noise [14], see example of acquired antenna signal in Fig. 3. There are various sources of this background noise. Noise signal can be generated by radio broadcasting, atmospheric disturbs, switching power supplies or by other types of discharges. According to the influence of background noise on the frequency spectrum and time domain of acquired signals, most noise signals in observed data can be separated into two groups: discrete spectral interference (DSI) and random pulses interference (RPI) [15].

A. Discrete Spectral Interference (DSI)

Noise signals in this group have usually a narrow frequency spectrum [16], the most common sources of this noise in acquired signals are radio broadcast transmitters [17]. During DSI presence, PD pattern pulses are modulated on a DSI noise signal. This effect significantly decreases the ratio of PD pattern/noise amplitudes. DSI noise with high amplitude can cover PD pattern in a signal, making it impossible to detect according to its amplitude.

Radio waves in the range of the examined frequency spectrum (up to 10 MHz) are propagated through the groundwave and skywave. Thus, the amplitude of this noise is highly variable and depends on many factors, such as the actual season of the year and daytime, weather conditions, etc. [18]. Fig. 4 is a graph with two lines of RMS values of background noise amplitude in the examined frequency spectrum. This graph is based on the data from two randomly chosen days. The impact of solar

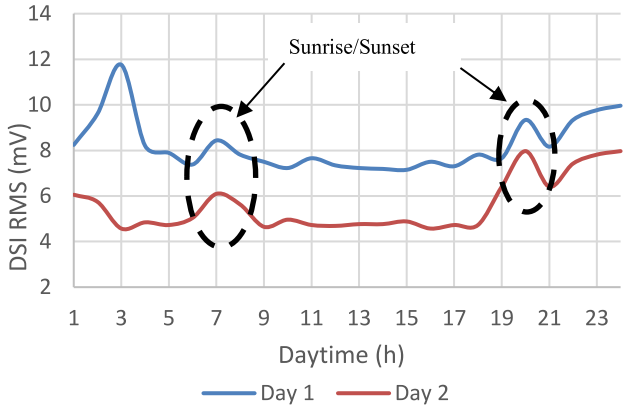

Fig. 4. The influence of gray-line propagation.

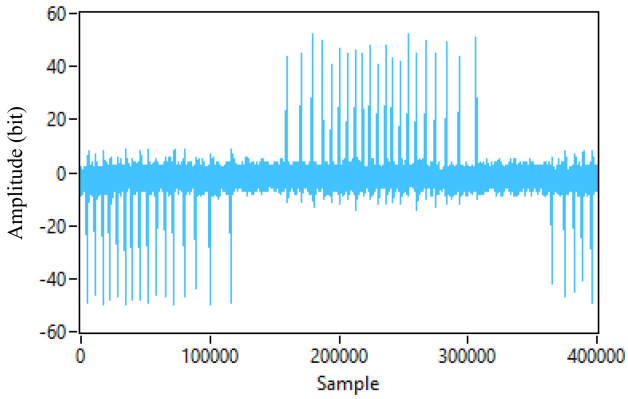

Fig. 5. Example of acquired RPI pulses.

activity is clearly visible, DSI background noise is higher during the night-time.

There is also significant increase of DSI amplitude during sunrise and sunset. This is caused by so called gray-line propagation of radio waves [19], where twilight zone in atmosphere acts as a wave guide.

B. Random Pulse Interference (RPI)

This interference is caused by any CC non-relative pulse appearance in the examined signal. The origin of such pulses varies. They can be caused by lightning, switching operations or by electric discharges. RPI is wideband type of interference [20].

Example of such situation is in Fig. 5. This pattern was acquired during open state of the disconector. Open state of this recloser triggeres PD in it. Those PD are not related to CC, but to the floating voltage electrodes in the disconector. Such type of PD can be easily recognized, because it creates a typical "pulse train", which contains pulses of a similar amplitude with almost uniform spacing, representing defined repetetive sequences of pulses [21]. Generally, RPI noise creates peaks in time domain of the signal, which can be misinterpreted as CC related pulses.

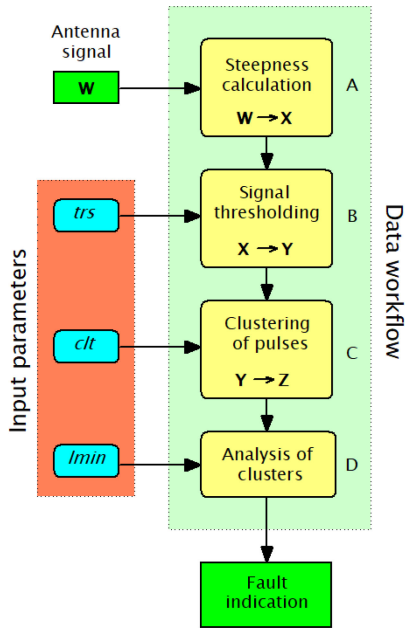

Fig. 6. Diagram of the algorithm workflow.

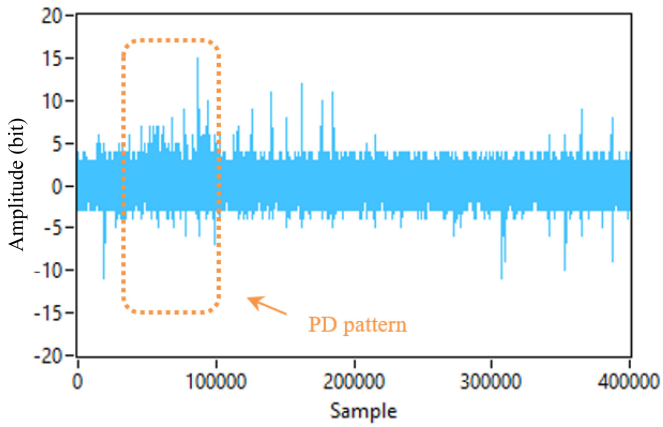

Fig. 7. Acquired signal with PD pattern during fault state (vector **W**).

V. Classification Algorithm

For an automatic PD pattern detection, a simple algorithm was created to classify the acquired data. This algorithm is based on the knowledge of the examined signals. The algorithm works in four steps (Fig. 6). In the first step (A), signal to noise ratio is increased. The second step (B) removes DSI noise, the third step (C) removes RPI noise. In the last step (D), PD pattern is detected. Only three parameters are needed to set the algorithm.

Input data for the classification is the time series of samples of acquired signal from the antenna output. This input signal is represented by the vector **W**. Fig. 7 gives an example of a raw acquired signal from antenna output. This signal was acquired during a fault state of the overhead line and it contains a PD pattern, DSI and RPI noise. The signal was chosen as an example to describe the algorithm workflow.

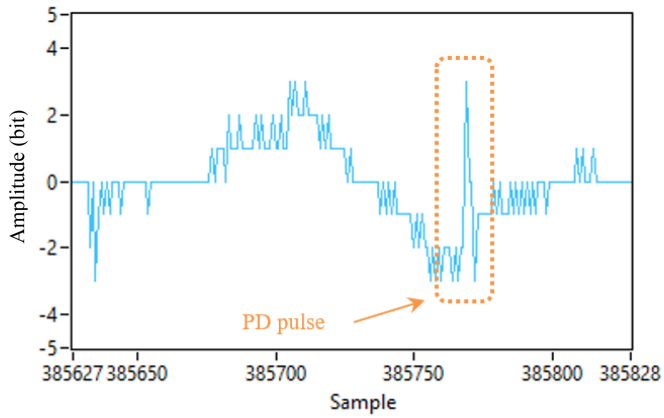

Fig. 8. PD pattern pulse buried in DSI noise (vector **W**).

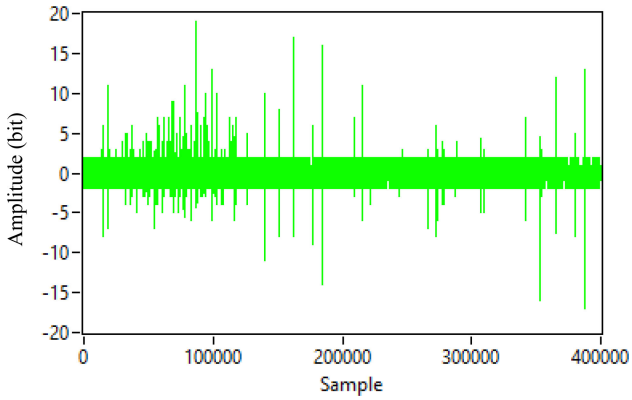

Fig. 9. Vector of steepness (**X**).

A. *Steepness Calculation*

First of all, the input vector **W** (Fig. 7) is transformed into the vector of steepness **X** (Fig. 9). In this step, steepness of every rising and falling edge in the input signal is calculated. The edge detection is based on a change of a polarity of the difference between two following samples. For example, when falling edge turns into a rising edge, polarity of the difference changes from negative to positive, and vice versa. Timestamp, where the polarity of a difference changes, determines the edge (points l and f). The first (w_f) and the last (w_l) element of the edge is then used for steepness calculation according to equation (1).

$$x\,(i = l) = \frac{w_f - w_l}{l - f} \tag{1}$$

The reason for this transformation is the DSI noise. The amplitude of DSI is sometimes higher than amplitude of the PD pulse itself, so it cannot be distinguished in the signal according to its amplitude (see example of this situation in Fig. 8).

In such a case, the PD pattern is modulated in DSI noise and it is complicated to detect it. Steepness of the PD pulse is usually much higher than steepness of DSI. This is why PD pulse is more visible after this transformation, it increases the PD pattern signal to DSI ratio (compare Fig. 7 with Fig. 9).

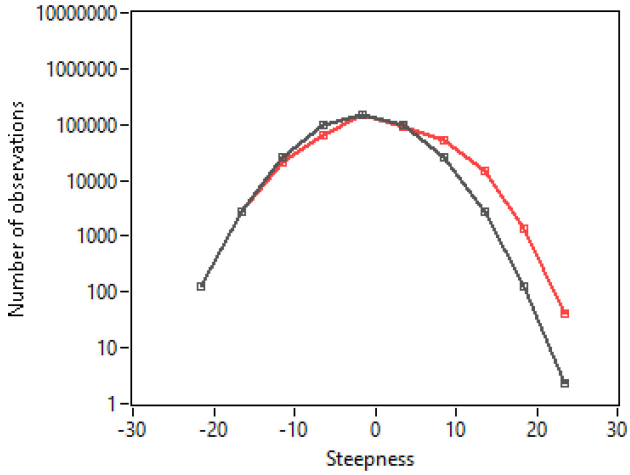

Fig. 10. Probability distribution of elements of vector **X** (red curve) during no-fault state (black curve = normal deviate).

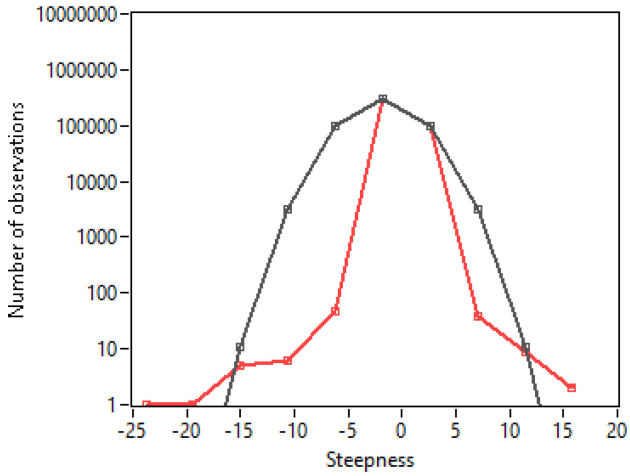

Fig. 11. Probability distribution of elements of vector **X** (red curve) during HIF (black curve = normal deviate).

B. *Signal Tresholding*

In the next step, threshold is applied on the vector **X** to remove DSI. Fixed thresholding is not suitable for this application, because of the variable amplitude of DSI (see Fig. 4). A fixed threshold value must be set according to the worst background noise scenario. But such a high value of threshold will significantly decrease the range of detection during quiet times. Therefore, soft thresholding is used in this algorithm.

When elements of input data contain only background DSI noise, the distribution of all elements of vector **X** is similar to normal distribution (Fig. 10).

Most of the PD or RPI pulses are not within normal deviate, as it was observed in acquired data (Fig. 11).

To distinguish between DSI and PD/RPI pulses, Z-score test is used. This test analyses the normality of probability distribution of the vector elements. For each element of the vector **X** (Fig. 9),

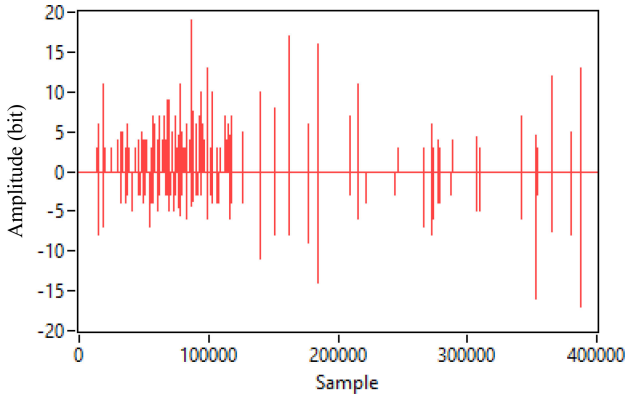

Fig. 12. Vector of thresholded steepness (**Y**).

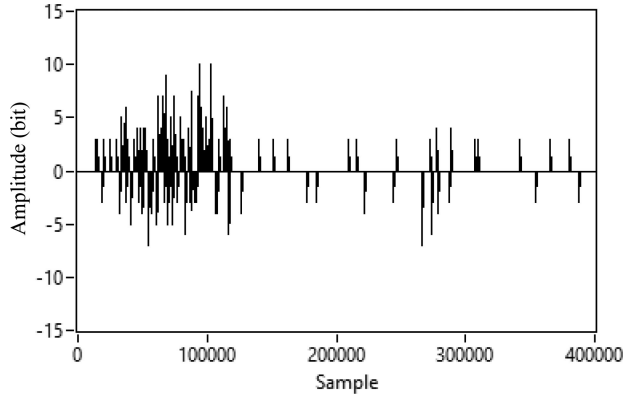

Fig. 13. Vector of clusters (**Z**).

z-score parameter is calculated according to equation:

$$Z\_scor\ e_i = \frac{|x_i| - \mu}{\sigma} \tag{2}$$

where mean μ is the average value of the vector X elements and population standard deviation σ represents the elements dispersion.

For normal probability distribution, maximal value of z-score is usually lower than 3 [22]. Z-score of an element is compared with the parameter *trs*. Only elements of the vector with *Z_score* value above the *trs* are transferred to the next step, as elements of a vector **Y** (Fig. 12). This vector **Y** contains only RPI and PD pulses, DSI is eliminated.

Soft thresholding, based on z-score parameter, is automatically self-adapted according to DSI amplitude. With increasing DSI amplitude (y_i), standard deviation σ is also increased (see Eq. 2), so their ratio is similar and there is no negative influence of variable DSI amplitude on the thresholding function. μ value in Eq. 2 is close to zero for most of the acquired signals, so it does not have any influence at all. RPI and PD pulses do not affect the standard deviation of vector **X**, because the number of these pulses is insignificant compared to the number of all elements in this vector.

C. Clustering of Pulses

In the third step, spacing of non-zero elements in the vector **Y** is examined. The distance between each neighbouring non-zero elements is calculated. Group of these elements with spacing smaller than *clt* parameter is considered as a cluster and it is transferred into vector **Z** (Fig. 13). This eliminates RPI pulses from the signal, because the spacing of RPI pulses is greater than *clt* parameter.

D. Analysis of Clusters

In the last step, the length of every single cluster in the vector **Z** is examined. If the length of any cluster is bigger than parameter *lmin*, pulses in the cluster are considered as PD pattern pulses. In such a case, the input signal is classified as PD positive.

As it can be seen in Fig. 14, a portion of PD pattern in input signal **X** was correctly detected by the algorithm as a PD pattern.

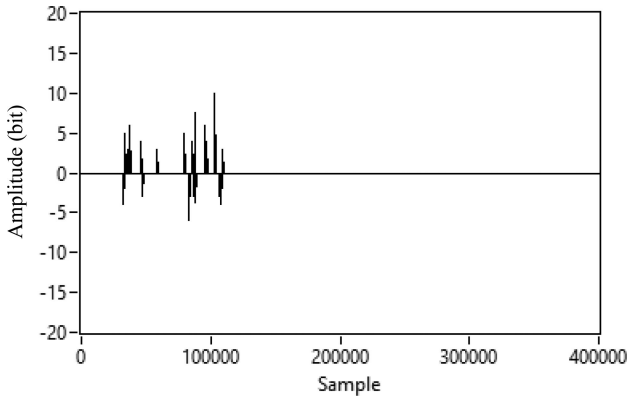

Fig. 14. Detected part of PD pattern in clusters of vector **Z.**

TABLE I
INPUT PARAMETERS OF THE ALGORITHM

trs	*clt*	*lmin*
4	2000	9000

VI. EXPERIMENT RESULTS

During the operation of the antenna sensor, we created a dataset of signals. It contains 26660 signals acquired during various conditions of the overhead line and various background noise amplitudes. Due to the low fault rate of the examined overhead line, only 200 signals from the dataset were acquired during HIF, when a vegetation was in the direct contact with CC. Three input parameters of the algorithm were set according to Table I.

Input parameters were set experimentally. After the acquisition of the first several fault states signals, input parameters were set by the bisection method for the best detection results (e.g. the biggest difference between *recall* and accuracy *values*).

All acquired signals were classified by the algorithm. The result of the classification can be seen in Table II.

Data cross validation were used to quantify the quality of detection [23]. All acquired data were used, no matter how many pulses signal consisted. Precision, accuracy and recall

TABLE II
CLASSIFICATION RESULTS

Signal classification	Description	Number of signals
t_p (true positive)	• PD pattern is present • PD pattern is detected	100
t_n (true negative)	• PD pattern is not present • PD pattern is not detected	26 440
f_p (false positive)	• PD pattern is not present • PD pattern is detected	20
f_n (false negative)	• PD pattern is present • PD pattern is not detected	100

TABLE III
DATA CROSS VALIDATION RESULTS

	Accuracy	*Precision*	*Recall*
Proposed method	99.5 %	83.3 %	50 %
SLI method	99.8 %	95.2 %	68.4 %

were calculated according to equations:

$$Accuracy : \frac{t_p + t_n}{t_p + t_n + f_p + f_n} \tag{3}$$

$$Precision : \frac{t_p}{t_p + f_p} \tag{4}$$

$$Recall : \frac{t_p}{t_p + f_n} \tag{5}$$

Because the main motivation for this experiment was to replace SLI sensors with antenna, results of detection were compared with current SLI method. Algorithm of compared SLI method is described in [24].

As it is clear form data cross validation results, the algorithm classified 99.5% of acquired antenna sensor signals correctly. When PD pattern was presented in a signal, it was classified correctly in 83.3% cases. But it was able to detect only 50% of all recorded PD patterns in the dataset.

There are various reasons why 50% of positive signals where incorrectly classified by the algorithm as negative. Most of this false negative HIF were caused by almost dry brunches, where the number of PD pulses in acquired signal is very low. Other false negative HIF were situated in a large distance from the detector, where significant number of pulses was buried in DSI noise.

From the point of overhead line operation, the accuracy and the precision are the most important parameters. These parameters describe the possibility of false hit appearance and it is necessary to keep the number of false hits events as low as possible. In the opposite case of high false hit rate occurrence, the maintenance workers will start to ignore the output signalization of the detector.

Low recall value is not as significant issue as it appears to be. The partial discharges activity has a long-term presence. It usually takes from several hours to several weeks to severely damage the insulation. Thus, even with low recall value, the detector will sooner or later detect the presence of HIF appearance.

VII. CONCLUSION

All the tested data were gathered from overhead line in a real environment during its regular operation. This enabled us to create a unique dataset of signals with various kinds of noise. This cannot be achieved in a laboratory environment. With the detailed knowledge of background noise properties, we were able to design a simple algorithm for PD pattern detection in acquired antenna signals. There are only three input parameters for algorithm, which makes it easily adaptable according to the local noise condition.

It is hard to estimate the range of distance of treefall and branch detection. Intensity of PD activity strictly depends on the level of the fallen branch or tree humidity. A fresh branch with sap inside can be detected on a distance of several kilometers. Contact of a CC with dead and already dried branch/tree cannot be detected by any of the PD based methods, because it does not trigger PD activity. Variable amplitude of background noise also plays an important role in the maximum possible range of detection. All recorded HIFs in dataset were within the range of 1 km from the detector.

The proposed method for the isolation of fault detection of CC on MV does not provide as good results as SLI method yet. Unlike the SLI method, it cannot evaluate the type of fault (phase-phase or phase-ground) or determine the affected phase(s). But it has its advantages. It is significantly cheaper, so it can be installed in a large number to provide optimal fault localization. Simple algorithm does not require a high computing power. Another advantage of described method is the possibility of antenna sensor installation on the overhead line during its operation, without the necessity of overhead line disconnection. The dataflow from antenna sensor is significantly smaller when compared to SLI sensors (only one antenna sensor is necessary for the detector operation instead of three SLI sensors). This enables us to reduce the time of data transmission, which is at this moment the limiting factor for minimal possible period between two following measurements.

In the next phase of our research, we will focus on tests of different types of antenna sensors. Until now, we have used an antenna from the market. Now, we would like to design our own antenna, especially for the purpose of PD detection. The most limiting factor is in this case the maximal dimensions of antenna, because it is mounted in the buffer zone of overhead line. For the examined frequency band, any type of antenna is extremely short compared to the wavelength of the signals within the measuring range of the DAQ (below 10 MHz). Another task is to improve the classification algorithm to make it more noise resistant and accurate. Especially RPI is problematic, because it generates false hits in classification. We would like to enhance the algorithm with other de-noising methods and thus, improve the classification of acquired signals from the antenna sensor.

REFERENCES

[1] P. Pakonen, "Detection of incipient tree faults on high voltage covered conductor lines," Ph.D. dissertation, Tampere Univ. Technol., Tampere, Finland, 2007.

[2] G. Eduful and K. N. Asante, "In search of electric power reliability in forested terrain with covered conductors," in *Proc. 4th Int. Conf. Adaptive Sci. Technol.*, 2012, pp. 149–153.
[3] D. P. S. Gomes and C. Ozansoy, "High-sensitivity vegetation high-impedance fault detection based on signal's high-frequency," *IEEE Trans. Power Del.*, vol. 33, no. 3, pp 1398–1407, Jun. 2018.
[4] A. Ghaderi, H. A. Mohammadpour, H. L. Ginn, and Y. Shin, "High-impedance fault detection in the distribution network using the time-frequency-based algorithm," *IEEE Trans. Power Del.*, vol. 30, no. 3, pp. 1260–1268, Jun. 2015.
[5] P. Pakonen, "Characteristics of partial discharges caused by trees in contact with covered conductor lines," *IEEE Trans. Dielectrics Elect. Insul.*, vol. 15, no. 6, pp. 1626–1633, Dec. 2018.
[6] W. Zhang, Z. Hou, H. Li, C. Liu, and N. Ma, "An improved technique for online PD detection on covered conductor lines," *IEEE Trans. Power Del.*, vol. 29, no. 2, pp. 972–973, Apr. 2014.
[7] M. Isa, G. M. Hashmi, and M. Lehtonen, "Comparative study of on-line three phase PD monitoring systems for overhead covered conductor distribution lines," in *Proc. 44th Int. Universities Power Eng. Conf.*, 2009, pp. 1–5.
[8] K. J. Khor and K. L. Wong, "Partial discharge sensing in overhead distribution line," in *Proc. Australas. Universities Power Eng. Conf.*, 2008, pp. 1–5.
[9] G. A. Hussain, L. Kumpulainen, M. Lehtonen, M. Hashmi, and M. Shafiq, "Signal processing of PD measurements to predict arcing faults in MV switchgears," in *Proc. IEEE Int. Conf. Ind. Technol.*, 2013, pp. 916–921.
[10] J. L. Ten and H. Zhu, "On-line PD detection in XLPE power cable based on fractal theory," in *Proc. IEEE/PES Transmiss. Distribution Conf. Exhib.*, 2006, pp. 592–595.
[11] H. Chunguang, F. Weidong, H. Ying and C. Yundong, "Research on PD detection of 12 kV switchgear based on fuzzy logic algorithm," in *Proc. 4th Int. Conf. Elect. Power Equip. - Switching Technol.*, 2017, pp. 843–846.
[12] M. Krátký, S. Mišák, P. Gajdoš, P. Lukáš, R. Bača, and P. Chovanec, "A novel method for detection of covered conductor faults in medium voltage overhead line systems," *IEEE Trans. Ind. Electron.*, vol. 65, no. 1, pp. 543–552, Jan. 2018.
[13] S. Mišák, J. Fulneček, T. Jezowicz, T. Vantuch, and T. Buriánek, "Usage of antenna for detection of tree falls on overhead lines with covered conductors," *Adv. Elect. Electron. Eng.*, vol. 15, no. 1, pp. 21–27, Mar. 2017.
[14] C. Ma, H. Li, W. Zhou, and J. Yu, "Background noise of partial discharge detection and its suppression in complex electromagnetic environment," in *Proc. IEEE Int. Conf. High Voltage Eng. Appl.*, 2018, pp. 1–4.
[15] H. Zhang, T. R. Blackburn, B. T. Phung, and D. Sen, "A novel wavelet transform technique for on-line partial discharge measurements 2. On-site noise rejection application," *IEEE Trans. Dielectrics Elect. Insul.*, vol. 14, no. 1, pp. 15–22, Feb. 2007.
[16] V. Nagesh and B. I. Gururaj, "Evaluation of digital filters for rejecting discrete spectral interference in on-site PD measurements," *IEEE Trans. Dielectrics Elect. Insul.*, vol. 28, no. 1, pp. 73–85, Feb. 1993.
[17] The European table of frequency allocations and applications in the frequency range 8.3 kHz to 3000 GHz, Electronic Communications Committee, Oct. 2018. [Online]. Available: https://www.ecodocdb.dk/download/2ca5fcbd-4090/ERCREP025.pdf
[18] C. Haslet, "Atmospheric effects," in *Essentials of Radio Wave Propagation*, 1st ed., Cambridge, U.K.:Cambridge Univ. Press, 2008, pp. 116–148.
[19] E. Callaway, "Gray Line Propagation, or Florida to Cocos (Keeling) on 80m," in *Proc. QEX*, Nov./Dec. 2016, pp. 19–26. [Online]. Available: http://www.arrl.org/files/file/QEX%20Binaries/2016/Callaway.pdf
[20] S. Winder and J. Carr, "Propagation of radio waves," in *Newness Radio and RF Engineering Pocket Book*, 1st ed. New York, NY, USA: Elsevier, 2002, pp. 1–25.
[21] S. A. Madhar, P. Mraz, A. R. Mor, and R. Ross, "Physical interpretation of the floating electrode defect patterns under AC and DC stress conditions," *Elect. Power Energy Syst.*, vol. 118, pp. 1–8, Dec. 2020.
[22] K. Viswanathan, L. Choudur, V. Talwar, C. Wang, G. Macdonald and W. Satterfield, "Ranking anomalies in data centers," in *Proc. IEEE Netw. Oper. Manage. Symp.*, 2012, pp. 79–87.
[23] R. Kohavi, "A study of cross-validation and bootstrap for accuracy estimation and model selection," in *Proc. Int. Joint Conf. Artif. Intell.*, 1995.
[24] S. Mišák, J. Fulneček, T. Vantuch, T. Buriánek, and T. Ježowicz, "A complex classification approach of partial discharges from covered conductors in real environment," *IEEE Trans. Dielectrics Elect. Insul.*, vol. 24, no. 2, pp. 1097–1104, Apr. 2017.

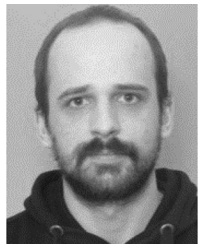

Jan Fulneček was born in Karviná in the Czech Republic, in 1989. He received the Ph.D. degree in 2018 from the Technical University of Ostrava, Department of Electrical Power Engineering.

Currently, he works as a Junior Researcher at the ENET research Centre and as Assistant Professor at the Department of Electrical Power Engineering, VŠB Technical University of Ostrava. His research interests are in the area of electrical equipment diagnostics.

Stanislav Mišák was born in Slavičín in the Czech Republic, in 1978. He received the, Ing. and Ph.D. degrees in 2003 and 2007, respectively, from the Department of Electrical Engineering, VŠB – Technical University of Ostrava, where he is currently Professor and Director of the research centre ENET. He holds a patent for a fault detector for medium voltage overhead lines. His current work includes the implementation of smart grid technologies using prediction models and bio–inspired methods.